

## Effect of the Anode-to-Cathode Distance on the Electrochemical Reduction in a LiCl-Li<sub>2</sub>O Molten Salt

Eun-Young Choi\*, Hun-Sook Im, and Jin-Mok Hur

Korea Atomic Energy Research Institute, Daedok-daero 989-111, Yuseong-gu, Daejeon 305-353, Republic of Korea

(Received July 17, 2013 : Accepted July 30, 2013)

**Abstract :** Electrochemical reductions of UO<sub>2</sub> at various anode-to-cathode distances (1.3, 2.3, 3.2, 3.7 and 5.8 cm) were carried out to investigate the effect of the anode-to-cathode distance on the electrochemical reduction rate. The geometry of the electrolysis cell in this study, apart from the anode-to-cathode distance, was identical for all of the electrolysis runs. Porous UO<sub>2</sub> pellets were electrolyzed by controlling a constant cell voltage in molten Li<sub>2</sub>O-LiCl at 650°C. A steel basket containing the porous UO<sub>2</sub> pellets and a platinum plate were used as the cathode and anode, respectively. The metallic products were characterized by means of a thermogravimetric analyzer, an X-ray diffractometer and a scanning electron microscope. The electrolysis runs conducted during this study revealed that a short anode-to-cathode distance is advantageous to achieve a high current density and accelerate the electrochemical reduction process.

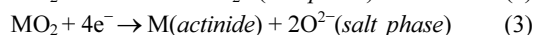
**Keywords :** Electrochemical reduction, Uranium oxide, Uranium, Li<sub>2</sub>O-LiCl molten salt

### 1. Introduction

The FFC (Fray-Farthing-Chen) Cambridge process has been regarded as an innovative method for the electrochemical reduction of solid oxides into their metals because it is simple, cost-effective, and environmentally friendly. Ever since the direct reduction of TiO<sub>2</sub> to titanium metal in a molten salt electrolysis cell was demonstrated in the first report on the FFC process,<sup>1)</sup> the application of the process has been expanded to the reduction of the various metal oxides such as SiO<sub>2</sub>,<sup>2)</sup> Ta<sub>2</sub>O<sub>5</sub>,<sup>3)</sup> Fe<sub>2</sub>O<sub>3</sub>,<sup>4)</sup> SnO<sub>2</sub>,<sup>5)</sup> Tb<sub>4</sub>O<sub>7</sub>,<sup>6)</sup> Nb<sub>2</sub>O<sub>5</sub>,<sup>7-9)</sup> Cr<sub>2</sub>O<sub>3</sub>,<sup>10,11)</sup> and CeO<sub>2</sub>.<sup>12)</sup> In particular, the electrochemical reduction of spent oxide fuel (mainly consisting of UO<sub>2</sub>) to a metallic form has been successfully employed in pyroprocessing technology for the closed nuclear fuel cycle.<sup>13,14)</sup> Pyroprocessing based on molten salt electrolysis is one of the key technologies for reducing the amount of spent nuclear fuel and destroying toxic waste products, such as the long-life fission products in spent nuclear fuels. During pyroprocessing, the

electrorefining process that is used to separate and recover uranium, plutonium and other actinides in molten chloride media cannot accept the spent oxide fuel directly, because the actinide oxides are not dissolved in the chloride salt. Thus, the electrochemical reduction of the spent oxide fuel to a metallic form is a head-end step of the electrorefining process.<sup>15-29)</sup>

In the electrochemical reduction process, oxides fuels are loaded at the cathode in molten LiCl so as to dissolve oxide ions. The cathode reactions are as follows<sup>1)</sup>:

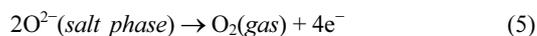


Li<sub>2</sub>O produced by reaction (2) in molten LiCl is dissociated into Li<sup>+</sup> and O<sup>2-</sup>:



When a platinum anode is employed, oxygen ions are oxidized to produce oxygen gas on the anode surface, as follows:

\*E-mail: eychoi@kaeri.re.kr



When an electrical potential is applied, the actinide metal oxide is reduced to metal and remains at the cathode. The oxygen ion ( $\text{O}^{2-}$ ) produced at the cathode is transported through the salt and discharges at the anode to form  $\text{O}_2$  gas.  $\text{Li}_2\text{O}$  is initially added to molten  $\text{LiCl}$  to speed up the electrochemical reaction and prevent the anodic dissolution of the platinum. The diffusion of  $\text{O}^{2-}$  ions from the inside of the oxide fuel to the anode surface via the bulk salt determines the reduction rate during electrolysis.<sup>20,30-33)</sup>

The commercialization of the electrochemical reduction process can be expedited if a more efficient electrolysis cell can be designed for a large-scale production. Determining configuration, capacity, size and material of the cell is essential to design a scaled-up electrochemical reduction process. The cell configuration includes the heat shields, the location of the electrodes, the shape of the cathode and anode, the anode shroud, the anode/cathode surface area ratio, the gas outlet at the anode, and the anode-to-cathode distance. Many researchers have tried to increase the efficiency of electrochemical processes by considering the influence of the anode-to-cathode distance.<sup>34-37)</sup> Kasherman and Skyllas-Kazacos<sup>34)</sup> investigated the effect of the anode-to-cathode distance on the cell potential and electric bath resistivity in the Hall-Heroult process for aluminum production in molten salt bath.

In the electrochemical reduction process of metal oxide for its metal production in molten salt, it was has been predicted that a short anode-to-cathode distance will be advantageous to improve the energy efficiency.<sup>38,39)</sup> However, the effect of the anode-to-cathode distance on the electrochemical reduction process has not experimentally verified thus far. In this study, electrochemical reductions of porous  $\text{UO}_2$  pellets were carried out in a molten  $\text{Li}_2\text{O-LiCl}$  salt at various anode-to-cathode distances (1.3, 2.3, 3.2, 3.7 and 5.8 cm) and their reduction rates were compared.

## 2. Experimental

### 2.1. Materials

Anhydrous  $\text{LiCl}$  (99.5% purity, Alfa Aesar) and  $\text{Li}_2\text{O}$  (99.5% purity, Alfa Aesar) were used as the electrolytes. The  $\text{LiCl}$  salt was dehydrated and kept in

an Ar glove box beforehand. The porous  $\text{UO}_2$  pellets were prepared as follows: After mixing  $\text{U}_3\text{O}_8$  powder with 0.2 wt.% of N,N' ethylene bisstearamide (Sunkoo Ltd., Korea), we placed the mixture in cylindrical molds (with a diameter of 6 mm and a height of 8 mm) and pressed it into pellets with a pelletizer. Next we placed the cylindrical mixture in a furnace under a vacuum and heated it to  $700^\circ\text{C}$  at a heating rate of  $2^\circ\text{C}/\text{min}$ . This temperature was maintained for 1 h to remove the N,N' ethylene bisstearamide from the mixture. The remaining  $\text{U}_3\text{O}_8$  was heated to  $1350^\circ\text{C}$  at a heating rate of  $2^\circ\text{C}/\text{min}$ , and this temperature was maintained for 12 h to convert the  $\text{U}_3\text{O}_8$  to  $\text{UO}_x$  and to release the oxygen gas. Finally, the mixture was cooled to room temperature at a cooling rate of  $5^\circ\text{C}/\text{min}$ . The value of  $x$  in  $\text{UO}_x$  was determined by the potentiometric titration method to be 2.112. In this report, we refer to the prepared porous  $\text{UO}_{2.112}$  pellets simply as porous  $\text{UO}_2$  pellets.

### 2.2. Electrochemical reduction of $\text{UO}_2$

Fig. 1a shows a schematic of the cell used for the electrochemical reduction process. The electrolysis cell consists of a crucible, salt and a flange (a set of heat shields with ports), where the salt makes contact with the electrodes and probes. A photograph of the flange used for this study is presented in Fig. 1b. Figs 1c and 1d show its bottom and top, respectively. The small and round ports of the flange are for the reference electrode ((1) in Fig. 1d) and for salt

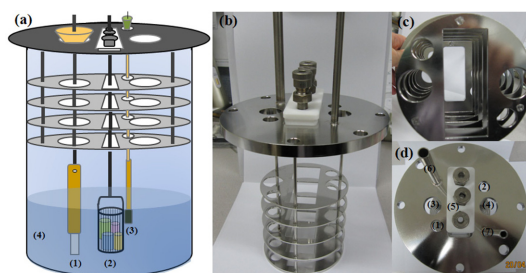


**Fig. 1.** (a) Schematic diagram of the electrochemical cell: (1) Pt anode with a MgO shroud, (2) cathode basket containing  $\text{UO}_2$  forms, (3) Li-Pb reference electrode and (4) 1 wt%  $\text{Li}_2\text{O-LiCl}$  molten salt, (b) photographs of the flange for the electrochemical cell, (c) bottom of the flange and (d) top of the flange; (1) for the reference electrode, (2) salt sampling, (3), (4), and (5) cathode or anode, (6) gas outlet and (7) gas inlet.

sampling ((2) in Fig. 1d), respectively. The rectangular port ((5) in Fig. 1d) and two adjacent ports ((3) and (4) in Fig. 1d) are for the anode and (or) cathode. Three screw joints are placed on the cover of the rectangular port, which can fix the rods of the anode or cathode. First, 800 g of LiCl was put in a stainless steel crucible (diameter, 95 mm) at room temperature. The reactor was heated to 650°C and maintained at that temperature. Then, 8.0 g of Li<sub>2</sub>O was fed into the reactor to reach the desired concentration. After the complete dissolution of Li<sub>2</sub>O, the electrodes were lowered into the molten salt. A liquid Li-Pb alloy (32 mol% Li) was used as a reference electrode. We placed 1 g of the Li-Pb alloy in an MgO tube with an inner diameter of 5 mm and a porous bottom. A tantalum wire (with a diameter of 0.5 mm) was then put into the tube and immersed in the liquid alloy for use as an electrical lead. A cylindrical cathode basket (20 mm in diameter) was surrounded with a 325 mesh sheet (sieve opening of 45 μm in size) to contain the UO<sub>2</sub> forms. Both the bottom and the mesh sheet of the basket were electrically conductive. In addition, we surrounded a 10 mm wide plate-type platinum (Pt) anode with an MgO shroud to provide a path for the oxygen gas produced on the anode surface. The exposed surface areas of the anode and cathode were constant. An Agilent E3633A power supply was used for the voltage control electrolysis process in order to reduce the UO<sub>2</sub>. The cathode potential during the electrochemical reduction was monitored with a digital multimeter (Agilent, 34405A). During the electrolysis run, the variation of the Li<sub>2</sub>O concentration in the molten salt was checked by a titration method, as follows. A molten salt sample of 0.4 g was taken from the reactor using a pipette and was dissolved in distilled water. The dissolved alkali solution was then titrated with 0.1 N HCl.

### 2.3. Characterization of metallic U reduced from UO<sub>2</sub>

After the experimental run, the reduced sample was rinsed with distilled water to remove the residual salt. The reduction conversion of UO<sub>2</sub> was determined by means of a thermogravimetric analyzer (TGA, TG/DTA 6300, Seiko Instruments Inc.). A 20 mg sample of metallic U was loaded into the Pt crucible for the TGA measurement and

heated to 600°C at a heating rate of 10°C/min in an air atmosphere. The surface morphology and the crystalline structure of the products were observed with a scanning electron microscope (SEM, Philips, XL-30) and a X-ray diffractometer (XRD, Rigaku MiniFlex), respectively.

### 3. Results and Discussion

The electrochemical reduction run was conducted with 29.9 g of P-55% in 1 wt% Li<sub>2</sub>O-LiCl molten salt at 650°C. The anode-to-cathode distance was 1.3 cm. Fig. 2 shows the electrolysis curves of (a) the cell voltage, (b) the current, and (c) the cathode potential as a function of time. The electrolysis run at a constant voltage (3.3 V) was interrupted at appropriate intervals, and the open circuit potential of the cathode was measured so that we could monitor the formation of lithium metal and prevent it from being deposited

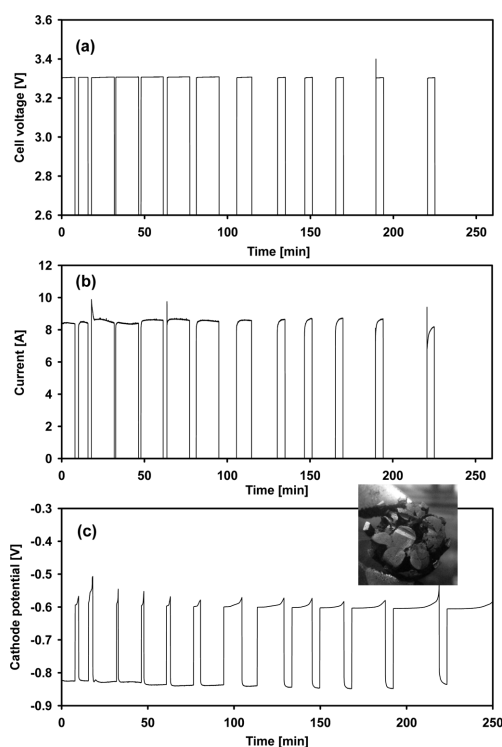


Fig. 2. Plots from the electrochemical reduction of UO<sub>2</sub> (29.9 g) in 1 wt% Li<sub>2</sub>O-LiCl at 650°C (the used anode-to-cathode distance used was 1.3 cm): (a) the cell voltage vs time, (b) the current vs time, and (c) the cathode potential vs time.

excessively on the cathode surface.<sup>32,33)</sup> The cathode potential was lowered to approximately  $-0.85$  V (Fig. 2c) by applying a cell voltage of  $3.3$  V (Fig. 2a) because a cyclic voltammetry test in our previous study<sup>40)</sup> showed that  $\text{UO}_2$  is reduced at a potential that is more negative than  $-0.60$  V. The  $\text{Li}/\text{Li}^+$  potential measured during the interruption of the electrolysis run was  $-0.60$  V against the  $\text{Li-Pb}$  reference electrode. The response current ranged from  $7.5$  to  $10$  A (Fig. 2b). This run was finally finished after  $137\%$  ( $16.3$  A h) of the theoretical electric charge had passed. The cathode basket was cut along the radial direction in a high-purity argon glove box. A photograph of a cross-section of the reduced pellets (inset of Fig. 2c) shows that  $\text{U}$  was metallic grey after a charge supply of  $150\%$ , unlike brown  $\text{UO}_2$ .

The crystalline structure of the fresh  $\text{UO}_2$  and the electrochemically reduced  $\text{UO}_2$  was compared by means of XRD. As shown Fig. 3a, the main sharp peaks, which can be assigned to  $\text{UO}_2$ , appear near  $2\theta = 33, 47, 56$  and  $69$ . On the other hand, in the XRD results of the reduced sample, the main sharp peaks of  $\text{UO}_2$  disappeared and new sharp peaks, which can be assigned to metallic uranium, appear at near  $2\theta = 36, 40, 51, 61,$  and  $65$  (Fig. 3b).<sup>41)</sup> These observations indicate that uranium oxide was successfully reduced to metallic uranium during the electrolysis process.

The microstructure of the fresh  $\text{UO}_2$  (Figs. 4a and 4b), and the electrochemically reduced  $\text{UO}_2$  (Figs. 4c and 4d) were compared by means of SEM. After the

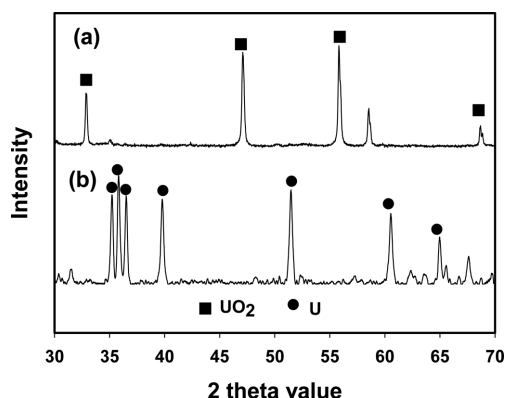


Fig. 3. XRD patterns: (a)  $\text{UO}_2$  before the electrochemical reduction and (b) metallic  $\text{U}$  after the supply of  $150\%$  of the charge.

electrolysis runs, it was observed that the particles were more connected and enlarged. In particular, the structure is sintered together and resembles a metal sponge with a nodular structure induced by the differences in the densities of the  $\text{UO}_2$  and metallic uranium.

The electrochemical reductions of  $\text{UO}_2$  at various anode-to-cathode distances were also conducted in a manner similar to that of the electrolysis run using anode-to-cathode distance of  $1.3$  cm (shown in Fig. 2). Various anode-to-cathode distances were used by placing the anode and cathode at different positions (ports, (3), (4) and (5) in Fig. 1d) in the flange top of the electrolysis cell. The positions of the anode and cathode for the various anode-to-cathode distances are presented in Fig. 5. The anode-to-cathode distances were measured at the closest distance between the anode and the cathode. All of the geometry factors of the electrolysis cell, in this case the position of the reference electrode, the height of the anode shroud, the direction of the anode plate, and the immersion height of the surfaces of the anode and cathode were identical except for the anode-to-cathode distances.

The results of the electrochemical reductions at various anode-to-cathode distances are given in Table 1. The mass of the  $\text{UO}_2$  used here was approximately  $29\sim 30$  g. The supply of the charge

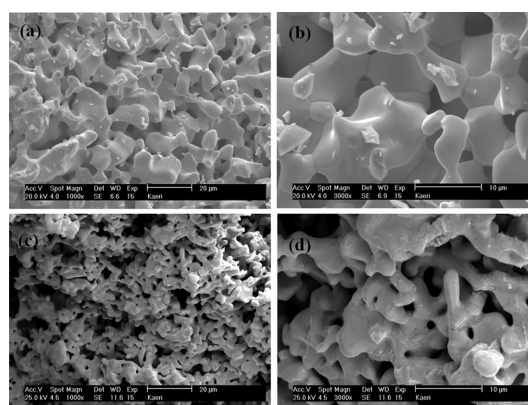
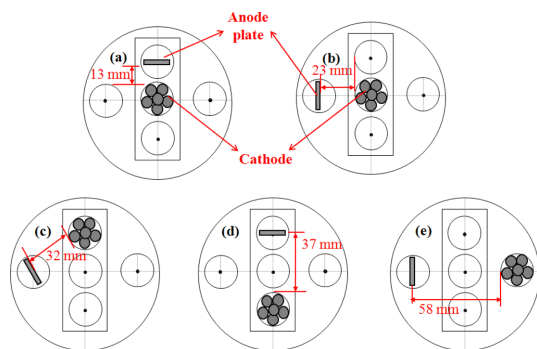


Fig. 4. Cross-sectional SEM images of  $\text{UO}_2$ : low-magnification view ( $1000\times$ ) (a) and high-magnification view ( $3000\times$ ), (b) before the electrochemical reduction process; low-magnification view ( $1000\times$ ) (c) and high-magnification view ( $3000\times$ ), (d) after the electrochemical reduction process.

**Table 1. The results of electrolysis runs of  $\text{UO}_2$  forms at various anode-to-cathode distances (constant voltage electrolysis - 3.3 V, in 1 wt%  $\text{Li}_2\text{O-LiCl}$  at  $650^\circ\text{C}$ )**

Anode-to-cathode distance [cm]	Mass of $\text{UO}_2$ [g]	Averaged current [A]	Electrolysis time [h]	Electric charge passed ( $Q$ )		Conversion rate to metal U [%] <sup>a</sup>
				A h	% <sup>a</sup>	
1.3	29.9	8.5	1.97	16.3	137	$94.5 \pm 3.2$
2.3	29.5	7.4	2.39	22.1	189	$92.1 \pm 4.5$
3.2	29.2	6.5	3.35	20.4	176	$91.0 \pm 5.0$
3.7	29.7	6.0	3.89	20.0	170	$99.0 \pm 0.5$
5.8	29.8	4.8	5.48	24.8	210	$61.5 \pm 5.2$

<sup>a</sup> Percent relative to the theoretical amount required to reduced all of the  $\text{UO}_2$  to metallic uranium



**Fig. 5. Various anode-to-cathode distances in the electrolysis cell using the configuration of the flange top, (a) 1.3 cm, (b) 2.3 cm, (c) 3.2 cm, (d) 3.7 cm and (e) 5.8 cm.**

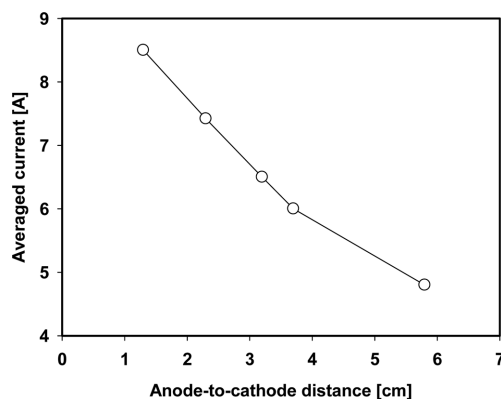


**Fig. 6. Averaged current measured at various anode-to-cathode distances during electrolysis.**

was terminated when the constant open circuit potential was maintained for a certain period of time, which resulted in the different electric charges passed for each run. The theoretical charges were calculated using the following equation<sup>33</sup>:

$$Q = 100q/[nF(w_{\text{UO}_2}/M_{\text{UO}_2})] \quad (6)$$

Here,  $n$  is the number of electrons involved in the cathode reaction (3),  $F$ , is the Faraday constant (26.8 A h/mol),  $w_{\text{UO}_2}$  is the weight of  $\text{UO}_2$  loaded in the cathode basket (g),  $M_{\text{UO}_2}$  is the molecular weight of  $\text{UO}_2$  (270.03 g/mol), and  $q$  is the electric charge passed for the electrolysis (A h). While 137% of the theoretical charge ( $Q$ ) was supplied for the electrolysis run using an anode-to-cathode distance of 1.3 cm, more than 170% of the theoretical charge was supplied for the other runs using longer anode-

to-cathode distances. For each electrolysis run, the averaged currents (the vacant dots) with the minimum and maximum values are plotted, as shown in Fig. 6. The maximum currents correspond to the initial sharp drop when cell voltage was newly applied after a certain period for the measurement of the open circuit potential. The sharp drop in the current may be due to the double layer charging period as shown in a previous publication.<sup>10</sup> The minimum currents correspond to the current measured in the vicinity of the end-point of the electrolysis run. These decreases in the current at the latter part of the electrolysis run result from a decrease in the reacting surface area of the metal oxide as the reduction of  $\text{UO}_2$  proceeds. In Table 1, as the anode-to-cathode distance increases, an increase in the electrolysis time caused by the decreased current was observed. It should be noted

that for the electrolysis run using an anode-to-cathode distance of 5.8 cm, the conversion rate of  $\text{UO}_2$  was only  $61.5 \pm 5.2\%$  whereas the conversion rates were more than 90% for the other runs using shorter anode-to-cathode distances. The achieved high current at the low anode-to-cathode distance can be explained by fast diffusion of  $\text{O}^{2-}$  ions from the cathode to the anode surface and less amounts of the Li metal and other contaminants. Li metal is generated by the reaction (1) and can exist excessively in the molten electrolyte especially at the latter part of the electrolysis run. Also, the molten LiCl may contain some conductive contaminants because a stainless steel was used as a material for the crucible and the cathode basket, which leads an electrical resistance especially at long anode-to-cathode distances. These results are consistent with the predictions in the previous study.<sup>38)</sup>

#### 4. Conclusions

The effect of the anode-to-cathode distance on the electrochemical reduction of  $\text{UO}_2$  has been examined in a molten  $\text{Li}_2\text{O-LiCl}$  at  $650^\circ\text{C}$ . Porous  $\text{UO}_2$  pellets of 29.0–30.0 g were separately electrolyzed at 1.3, 2.3, 3.2, 3.7 and 5.8 cm under an identical cell geometry condition. Successful conversions from  $\text{UO}_2$  to metallic U were achieved at 1.3, 2.3, 3.2, and 3.7 cm, showing a conversion rate of more than 91%. It was observed that the current decreased as the anode-to-cathode distance increased. For the electrolysis run using an anode-to-cathode distance of 5.8 cm, the conversion rate of  $\text{UO}_2$  was only 61.5%. The crucial aspect to the relationship between the current and the anode-to-cathode distance in the present study is that the predictions in the previous literatures were experimentally demonstrated. Moreover, this approach may be useful for design of an engineering-scale cell for the electrochemical reduction of metal oxides.

#### Acknowledgement

This work was supported by the Nuclear Research & Development Program of National Research Foundation (NRF) in a grant funded by the Korean Government.

#### References

1. G. Z. Chen, D. J. Fray, and T. W. Farthing, 'Direct electrochemical reduction of titanium dioxide to titanium in molten calcium chloride', *Nature*, **407**, 361 (2000).
2. K. Yasuda, T. Nohira, R. Hagiwara, and Y. H. Ogata, 'Direct electrolytic reduction of solid  $\text{SiO}_2$  in molten  $\text{CaCl}_2$  for the production of solar grade silicon', *Electrochim. Acta*, **53**, 106 (2007).
3. S. M. Jeong, J. Y. Jung, C. S. Seo, and S. W. Park, 'Characteristics of an electrochemical reduction of  $\text{Ta}_2\text{O}_5$  for the preparation of metallic tantalum in a  $\text{LiCl-Li}_2\text{O}$  molten salt', *J. Alloy Compd.*, **440**, 210 (2007).
4. S. I. Wang, G. M. Haarberg, and E. Kvalheim, 'Electrochemical behavior of dissolved  $\text{Fe}_2\text{O}_3$  in molten  $\text{CaCl}_2\text{-KF}$ ', *J. Iron Steel Res.*, **16**, 48 (2008).
5. M. Gibilaro, J. Pivato, L. Cassayre, L. Massot, L. P. Chamelot, and P. Taxil, 'Direct electroreduction of oxides in molten fluoride salts', *Electrochim. Acta*, **56**, 5410 (2011).
6. D. Wang, G. Qiu, X. Jin, X. Hu, and G. Z. Chen, 'Electrochemical metallization of solid terbium oxide', *Angew. Chem. Int. Ed.*, **45**, 2384 (2006).
7. X. Y. Yan and D. J. Fray, 'Production of niobium powder by direct electrochemical reduction of solid  $\text{Nb}_2\text{O}_5$  in a eutectic  $\text{CaCl}_2\text{-NaCl}$  melt', *Metall. Mater. Trans. B*, **33**, 685 (2002).
8. Q. Xu, L.-Q. Deng, Y. Wu, and T. Ma, 'A study of cathode improvement for electro-deoxidation of  $\text{Nb}_2\text{O}_5$  in a eutectic  $\text{CaCl}_2\text{-NaCl}$  melt at  $1073\text{K}$ ', *J. Alloy Compd.*, **396**, 288 (2005).
9. S. M. Jeong, H. Y. Yoo, J.-M. Hur, and C.-S. Seo, 'Preparation of metallic niobium from niobium pentoxide by an indirect electrochemical reduction in a  $\text{LiCl-Li}_2\text{O}$  molten salt', *J. Alloy Compd.*, **452**, 27 (2008).
10. G. Z. Chen, E. Gordo, and D. J. Fray, 'Direct electrolytic preparation of chromium powder', *Metall. Mater. Trans. B*, **35**, 223 (2004).
11. E. Gordo, G. Z. Chen, and D. J. Fray, 'Toward optimisation of electrolytic reduction of solid chromium oxide to chromium powder in molten chloride salts', *Electrochim. Acta*, **49**, 2195 (2004).
12. B. Claux, J. Serp, and J. Fouletier, 'Electrochemical reduction of cerium oxide into metal', *Electrochim. Acta*, **56**, 2771 (2011).
13. S. D. Herrmann, S. X. Li, M. F. Simpson, and S. Phongikaroon, 'Electrolytic reduction of spent nuclear oxide fuel as part of an integral process to separate and recover actinides from fission products', *Sep. Sci. Tech.*, **41**, 1965 (2006).
14. S. D. Herrmann and M. F. Simpson, 'Electrolytic reduction of spent light water reactor fuel: Bench-scale experiment results', *J. Nucl. Sci. Technol.*, **44**, 36 (2007).
15. J. L. Willit, W. E. Miller, and J. E. Battles, 'Electrorefining of uranium and plutonium - a literature review', *J. Nucl. Mater.*, **195**, 229 (1992).

16. J. J. Laidler, J. E. Battles, W. E. Miller, J. P. Ackerman, and E. L. Carls, 'Development of pyroprocessing technology', *Prog. Nucl. Energy*, **31**, 131 (1997).
17. R. W. Benedict and H. F. McFarlane, 'EBR-II spent fuel treatment demonstration project status', *Radwaste Magazine*, **5**, 23 (1998).
18. J. Serp., R. J. M. Konings, R. Malmbeck, J. Rebizant, C. Scheppler, and J.-P. Glatz, 'Electrochemical behavior of plutonium ion in LiCl-KCl eutectic melts', *J. Electroanal. Chem.*, **561**, 143 (2004).
19. K. M. Goff, J. C. Wass, K. C. Marsden, and G. M. Teske, 'Electrochemical processing of used nuclear fuel', *Nucl. Eng. Technol.*, **43**, 335 (2011).
20. S. M. Jeong, S.-B. Park, S.-S. Hong, C.-S. Seo, and S.-W. Park, 'Electrolytic production of metallic uranium from  $U_3O_8$  in a 20 kg-batch scale reactor', *J. Radioanal. Nucl. Chem.*, **268**, 349 (2006).
21. M. Iizuka, Y. Sakamura, and T. Inoue, 'Development of pyroprocessing and its future direction', *Nucl. Eng. Technol.*, **40**, 183 (2008).
22. J.-M. Hur, T.-J. Kim, I.-K. Choi, J. B. Do, S.-S. Hong, and C.-S. Seo, 'Chemical behavior of fission products in the petrochemical process', *Nucl. Eng. Technol.*, **162**, 192 (2008).
23. S. Kitawaki, T. Shinozaki, M. Fukushima, T. Usami, N. Yahagi, and M. Kurata, 'Recovery of U-Pu alloy from MOX using pyroprocess series', *Nucl. Technol.*, **162**, 118 (2008).
24. M. F. Simpson and S. D. Herrmann, 'Modeling the pyrochemical reduction of spent  $UO_2$  fuel in a pilot-scale reactor', *Nucl. Technol.*, **162**, 179 (2008).
25. J.-H. Yoo, C.-S. Seo, E.-H. Kim, and H. Lee, 'A conceptual study of pyroprocessing for recovering actinides from spent oxide fuels', *Nucl. Eng. Technol.*, **40**, 581 (2008).
26. K.-C. Song, H. Lee, J.-M. Hur, J.-G. Kim, D.-H. Ahn, and Y.-Z. Cho, 'Status of pyroprocessing technology development in Korea', *Nucl. Eng. Technol.*, **42**, 131 (2010).
27. Y. Sakamura and T. Omori, 'Electrolytic reduction and electrorefining of uranium to develop pyrochemical reprocessing of oxide fuels', *Nucl. Technol.*, **171**, 266 (2010).
28. H. Lee, G.-I. Park, K.-H. Kang, J.-M. Hur, J.-G. Kim, D.-H. Ahn, Y.-Z. Cho, and E. H. Kim, 'Pyroprocessing technology development at KAERI', *Nucl. Eng. Technol.*, **43**, 317 (2011).
29. K. M. Goff, R. W. Benedict, K. L. Howden, G. M. Teske, and T. A. Johnson, 'Pyrochemical treatment of spent nuclear fuel', *Proc. Global 2005*, p. 364, Tsukuba, Japan (2005).
30. J.-M. Hur, C. S. Seo, S. S. Hong, D. S. Kang, and S. W. Park, 'Metallization of  $U_3O_8$  via catalytic electrochemical reduction with  $Li_2O$  in LiCl molten salt', *React. Kinet. Catal. Lett.*, **80**, 217 (2003).
31. S. B. Park, B. H. Park, S. M. Jeong, J. M. Hur, C.-S. Seo, S.-H. Choi, and S. W. Park, 'Characteristics of an integrated cathode assembly for the electrolytic reduction of uranium oxide in a LiCl- $Li_2O$  molten salt', *J. Radioanal. Nucl. Chem.*, **268**, 489 (2006).
32. Y. Sakamura, M. Kurata, and T. Inoue, 'Electrochemical reduction of  $UO_2$  in molten  $CaCl_2$  or LiCl', *J. Electrochem. Soc.*, **153**, D31 (2006).
33. Y. Sakamura, T. Omori, and T. Inoue, 'Application of electrochemical reduction to produce metal fuel material form actinide oxides', *Nucl. Technol.*, **162**, 169 (2008).
34. D. Kasherman and M. Skyllas-Kazacos, 'Effects of anode-cathode distance on the cell potential and electrical bath resistivity in an aluminium electrolysis cell with a sloping  $TiB_2$  composite cathode', *J. Appl. Electrochem.*, **18**, 863 (1988).
35. D. H. Andersen and Z. L. Zhang, 'Study on the anode-to-cathode distance in an aluminum reduction cell', *Mater. Trans. B*, **42**, 424 (2011).
36. K. C. Pillai, S. J. Chung, and I.-S. Moon, 'Studies on electrochemical recovery of silver from simulated waste water from Ag(II)/Ag(I) based mediated electrochemical oxidation process', *Chemosphere*, **73**, 1505 (2008).
37. D. B. Gent, A. Wani, and A. K. Alshawabkeh, 'Experimental design for one dimensional electrolytic reactive barrier for remediation of munition constituent in groundwater', *Electrochim. Acta*, **86**, 130 (2012).
38. D. J. Fray, 'Emerging molten salt technologies for metals production. JOM. 53, 26-39. Allanore, A., Ortiz, L. A., Sadoway, D. R., 2011. Molten oxide electrolysis for iron production: identification of key process parameters for large scale development', *TMS Annual Meeting*, **121** (2001).
40. S. M. Jeong, H.-S. Shin, S.-S. Hong, J.-M. Hur, J. B. Do, and H. S. Lee, 'Electrochemical reduction behavior of  $U_3O_8$  powder in a LiCl molten salt', *Electrochim. Acta*, **55**, 1749 (2010).
41. J.-H. Hur, S. M. Jeong, and H. Lee, 'Underpotential deposition of Li in a molten LiCl- $Li_2O$  electrolyte for the electrochemical reduction of U from uranium oxides', *Electrochem. Commun.*, **12**, 706 (2010).